J|A|C|S
ARTICLES
Published on Web 02/20/2007

Ammonia Production at the FeMo Cofactor of Nitrogenase: Results from Density Functional Theory

Johannes Kästner*,† and Peter E. Blöchl*

Contribution from the Institute for Theoretical Physics, Clausthal University of Technology, D-38678 Clausthal-Zellerfeld, Germany

Received December 1, 2006; E-mail: J.Kaestner@dl.ac.uk; Peter.Bloechl@tu-clausthal.de

Abstract: Biological nitrogen fixation has been investigated beginning with the monoprotonated dinitrogen bound to the FeMo cofactor of nitrogenase up to the formation of the two ammonia molecules. The energy differences of the relevant intermediates, the reaction barriers, and potentially relevant side branches are presented. During the catalytic conversion, nitrogen bridges two Fe atoms of the central cage, replacing a sulfur bridge present before dinitrogen binds to the cofactor. A transformation from *cis*- to *trans*-diazene has been found. The strongly exothermic cleavage of the dinitrogen bond takes place, while the Fe atoms are bridged by a single nitrogen atom. The dissociation of the second ammonia from the cofactor is facilitated by the closing of the sulfur bridge following an intramolecular proton transfer. This closes the catalytic cycle.

1. Introduction

Nitrogen is an essential component of biological matter. However, despite the fact that nitrogen is the main part of our atmosphere, nature is in short supply of nitrogen. Molecular nitrogen is exceptionally inert, and only few bacteria have developed the ability to convert it into a form that can be further metabolized. Its inactivity is caused by the triple bond—one of the strongest covalent bonds. While high pressure and high temperature are required to convert N_2 into NH_3 in the industrial Haber−Bosch process, biological nitrogen fixation breaks the N−N triple bond at ambient conditions. For this purpose, nature employs the enzyme nitrogenase, one of the most complex bioinorganic catalysts in nature.

Nitrogenase converts N_2 into biologically accessible ammonia.[1−4] During the reaction, nonstoichiometric[5] amounts of hydrogen are produced

$$N_2 + (6 + 2x)H^+ + (6 + 2x)e^- \rightarrow 2NH_3 + xH_2$$

There is an ongoing dispute on whether or not there is a limiting stoichiometry of hydrogen production.[6] Often a limiting value of $x = 1$ is given, but also values smaller and larger than 1 have been reported.[7] Our theoretical calculations[8] support the view of a nonstoichiometric reaction.

Nitrogenase consists of two proteins: (1) the molybdenum−iron protein, which holds the active site, the FeMo cofactor (FeMoco), and (2) the iron protein which hydrolyzes MgATP and uses the obtained energy to provide the molybdenum−iron protein with electrons.

Kinetic studies of the mechanism of biological nitrogen fixation[9−12] indicate that the rate-limiting step of the reaction is the dissociation of the two proteins. In each of these association−dissociation cycles, one electron is transferred to the molybdenum−iron protein. The Fe protein transfers the electron from a Fe_4S_4 cluster to the so-called P cluster, Fe_8S_7, on the MoFe protein, from where it is passed on to the active site of the MoFe protein, the FeMo cofactor. Theoretical models[13,14] indicate that geometrical changes of the backbone of the Fe protein are responsible for using the energy from MgATP to transfer electrons to the MoFe protein.

The active center of the enzyme, shown in Figure 1, is the FeMoco, $MoFe_7S_9N$·homocitrate. The FeMoco is linked to the protein via two amino acid residues. While the structures of both proteins were resolved in 1992,[16−18] a central ligand of the FeMoco was found only recently.[15] Although the central ligand could be C, N, or O according to the X-ray analysis, the consensus among theoretical studies[19−21] is that nitrogen should

† Present address: Computational Science and Engineering Department, CCLRC Daresbury Laboratory, Daresbury, Warrington WA4 4AD, U.K.

(1) Burges, B. K. *Chem. Rev.* **1990**, *90*, 1377.
(2) Burges, B. K.; Lowe, D. J. *Chem. Rev.* **1996**, *96*, 2983.
(3) Eady, R. R. *Chem. Rev.* **1996**, *96*, 3013.
(4) Christiansen, J.; Dean, D. R.; Seefeldt, L. C. *Annu. Rev. Plant Physiol. Plant Mol. Biol.* **2001**, *52*, 269.
(5) Hadfield, K. L.; Bulen, W. A. *Biochemistry* **1969**, *8*, 5103.
(6) Rees, D. C.; Howard, J. B. *Curr. Opin. Chem. Biol.* **2000**, *4*, 559.
(7) Rivera-Ortiz, J. M.; Burris, R. H. *J. Bacteriol.* **1975**, *123*, 537.
(8) Kästner, J.; Blöchl, P. E. *Chem. Phys. Chem.* **2005**, *6*, 1724.
(9) Lowe, D. J.; Thorneley, R. N. F. *Biochem. J.* **1984**, *224*, 877.
(10) Thorneley, R. N. F.; Lowe, D. J. *Biochem. J.* **1984**, *224*, 887.
(11) Lowe, D. J.; Thorneley, R. N. F. *Biochem. J.* **1984**, *224*, 895.
(12) Thorneley, R. N. F.; Lowe, D. J. *Biochem. J.* **1984**, *224*, 903.
(13) Kurnikov, I. V.; Charnley, A. K.; Beratan, D. N. *J. Phys. Chem. B* **2001**, *105*, 5359.
(14) Liao, J. L.; Beratan, D. N. *Biophys. J.* **2004**, *87*, 1369.
(15) Einsle, O.; Tezcan, F. A.; Andrade, S. L. A.; Schmid, B.; Yoshida, M.; Howard, J. B.; Rees, D. C. *Science* **2002**, *297*, 1696.
(16) Kim, J.; Rees, D. C. *Nature* **1992**, *360*, 553.
(17) Kim, J.; Rees, D. C. *Science* **1992**, *257*, 1667.
(18) Georgiadis, M. M.; Komiya, H.; Chakrabarti, P.; Woo, D.; Kornuc, J. J.; Rees, D. C. *Science* **1992**, *257*, 1653.
(19) Hinnemann, B.; Nørskov, J. K. *J. Am. Chem. Soc.* **2003**, *125*, 1466.
(20) Lovell, T.; Liu, T.; Case, D. A.; Noodleman, L. *J. Am. Chem. Soc.* **2003**, *125*, 8377.
(21) Huniar, U.; Ahlrichs, R.; Coucouvanis, D. *J. Am. Chem. Soc.* **2004**, *126*, 2588.

 10.1021/ja068618h CCC: $37.00

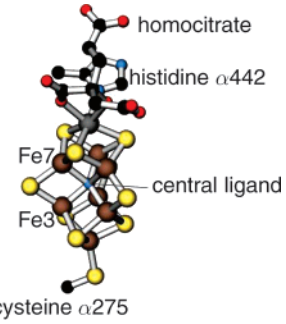

Figure 1. The FeMo cofactor of nitrogenase with its homocitrate ligand and the two residues linking the cofactor to the protein, histidine and cysteine. The experimental[15] geometry is shown.

be assigned as the central ligand. This result, however, is disputed due to an experiment[22] indicating that the central ligand might not be nitrogen. Our study rests on the assumption that the central ligand is nitrogen, even though we do not expect gross differences for isoelectronic replacements. The oxidation state of the resting state of the cofactor has been determined[20,23−25] to be $[MoFe_7S_9N]^0$ on the basis of the comparison of the theoretical results with various experimental findings. The so-called Thorneley−Lowe scheme provides insight into the first reduction steps, stating that N_2 binds after three or four electrons have been transferred to the MoFe protein, of which two reach the FeMoco.[26] Our calculations[25] indicate that each electron transfer is accompanied by a proton transfer to the FeMoco.

The question arises why nature employs a multicenter cluster as large as the FeMoco. The reaction mechanism has being studied for over 40 years, but the atomistic mechanism of substrate conversion at the FeMoco still remains an open issue.

The mechanisms for nitrogen fixation proposed up to now may be divided in two main groups, (1) conversion at Mo and (2) conversion at Fe. Theoretical studies of N_2 bound to Mo[27−31] are supported by a Mo-based model complex[32] that has been found to catalytically reduce N_2. Our own calculations, however, are not consistent with dinitrogen binding at the Mo site of the FeMo cofactor.[25,33] Numerous proposals have been made for reduction involving the Fe atoms. However, only the most recent ones take the central ligand into account. We discuss only those related to the present study. The direct way for N_2 is to bind head-on to Fe as studied by Nørskov's group.[34] In this study, the cofactor was found to serve solely as a binding site and did not play an "active" role in the reaction cycle. The axially bound dinitrogen is protonated until the first and then the second ammonia are dissociated. Sellmann et al.[35−38] were the first to suggest an opening of the cage, in analogy to that for smaller Fe complexes. In their model, two octahedrally coordinated low-spin Fe atoms positioned in close proximity bind dinitrogen between them, where it is reduced. Our calculations[25] support the view of a cage opening. In contrast to the previous model[35−38] based on cage opening, which leads to octahedrally coordinated Fe atoms, the Fe atoms in our model remain in a high-spin tetrahedral coordination, which points to a quite different chemistry. In our model, nitrogen binding is accompanied by the opening of a protonated sulfur bridge between two Fe sites, a process that balances the coordination number of the Fe site. In addition, this cage opening allows the formation of already two Fe−N bonds. These bonds labilize the triple bond of dinitrogen and, thus, activate dinitrogen for the first protonation.[33] Another proposal, by Huniar et al.,[21] also suggests opening of a sulfur bridge upon coordination of water to an Fe atom, complete protonation of the central ligand, and dissociation of ammonia. Then, N_2 inserts into the central cavity of the cofactor, where one nitrogen atom is fully protonated and dissociated, which closes the catalytic cycle. This intriguing proposal seems to be in conflict with isotope exchange (ESEEM/ENDOR) experiments[39] that exclude an exchange of a central nitrogen ligand.

We performed extensive density functional calculations to shed light on the catalytic cycle of dinitrogen reduction at the cofactor. A brief outline of the resulting mechanism has been given elsewhere.[8] A more detailed discussion of the docking of dinitrogen to the FeMoco and the first protonation of the bound dinitrogen have been given in two previous papers.[25,33]

Here, we provide a detailed discussion of the reaction steps leading from the protonated dinitrogen bound to the FeMoco via the cleavage of the dinitrogen bond and ammonia release to the closure of the catalytic cycle. In contrast to previous calculations, we not only determine the intermediates, but we also determine the relevant barriers and explore side reactions. Thus, we obtain a fairly comprehensive picture of the configuration space accessible by the reaction. In a similar approach, we were able to explain many experimental findings in the conversion of acetylene by nitrogenase.[40]

2. Computational Details

The cofactor of nitrogenase was modeled in analogy to our previous work on nitrogenase.[8,25,33,40] We performed DFT[41,42] calculations based on the projector-augmented wave[43,44] (PAW) method. The gradient-corrected PBE[45] functional was used for exchange and correlation. The planewave-based PAW method leads to the occurrence of periodic images of the structures. The electrostatic interactions between them were explicitly subtracted,[46] which results in gas-phase calculations. Wave function overlap was avoided by using a unit cell large enough to keep a distance of more than 6 Å between atoms of different periodic images. We used a planewave cutoff of 30 Ry for the auxiliary wave functions of the PAW method. The following shells were treated in

(22) Yang, T. C.; Maeser, N. K.; Laryukhin, M.; Lee, H. I.; Dean, D. R.; Seefeldt, L. C.; Hoffman, B. M. *J. Am. Chem. Soc.* **2005**, *127*, 12804.
(23) Dance, I. *Chem. Commun.* **2003**, 324.
(24) Vrajmasu, V.; Münck, E.; Bominaar, E. L. *Inorg. Chem.* **2003**, *42*, 5974.
(25) Schimpl, J.; Petrilli, H. M.; Blöchl, P. E. *J. Am. Chem. Soc.* **2003**, *125*, 15772.
(26) Fisher, K.; Newton, W.; Lowe, D. J. *Biochemistry* **2001**, *40*, 3333.
(27) Pickett, C. J. *J. Biol. Inorg. Chem.* **1996**, *1*, 601.
(28) Grönberg, K. L. C.; Gormal, C. A.; Durrant, M. C.; Smith, B. E.; Henderson, R. A. *J. Am. Chem. Soc.* **1998**, *120*, 10613.
(29) Szilagyi, R. K.; Musaev, D. G.; Morokuma, K. *Inorg. Chem.* **2001**, *40*, 766.
(30) Durrant, M. C. *Biochemistry* **2002**, *41*, 13934.
(31) Durrant, M. C. *Biochemistry* **2002**, *41*, 13946.
(32) Yandulov, D. V.; Schrock, R. R. *Science* **2003**, *301*, 76.
(33) Kästner, J.; Hemmen, S.; Blöchl, P. E. *J. Chem. Phys.* **2005**, *123*, 074306.
(34) Hinnemann, B.; Nørskov, J. K. *J. Am. Chem. Soc.* **2004**, *126*, 3920.
(35) Thorneley, R. N. F.; Lowe, D. J.; Dance, I.; Sellmann, D.; Sutter, J.; Coucouvanis, D.; Pickett, C. J. *J. Biol. Inorg. Chem.* **1996**, *1*, 575.
(36) Sellmann, D.; Utz, J.; Blum, N.; Heinemann, F. H. *Coord. Chem. Rev.* **1999**, *190*, 607.
(37) Sellmann, D.; Fürsattel, A.; Sutter, J. *Coord. Chem. Rev.* **2000**, *200*, 545.
(38) Kirchner, B.; Reiher, M.; Hille, A.; Hutter, J.; Hess, B. A. *Chem.—Eur. J.* **2005**, *11*, 574.
(39) Lee, H. I.; Benton, P. M. C.; Laryukhin, M.; Igarashi, R. Y.; Dean, D. R.; Seefeldt, L. C.; Hoffman, B. M. *J. Am. Chem. Soc.* **2003**, *125*, 5604.
(40) Kästner, J.; Blöchl, P. E. *Inorg. Chem.* **2005**, *44*, 4568.
(41) Hohenberg, P.; Kohn, W. *Phys. Rev.* **1964**, *136*, B864.
(42) Kohn, W.; Sham, L. J. *Phys. Rev.* **1965**, *140*, A1133.
(43) Blöchl, P. E. *Phys. Rev. B* **1994**, *50*, 17953.
(44) Blöchl, P. E.; Först, C. J.; Schimpl, J. *Bull. Mater. Sci.* **2003**, *26*, 33.
(45) Perdew, J. P.; Burke, K.; Ernzerhof, M. *Phys. Rev. Lett.* **1996**, *77*, 3865.
(46) Blöchl, P. E. *J. Chem. Phys.* **1995**, *103*, 7422.

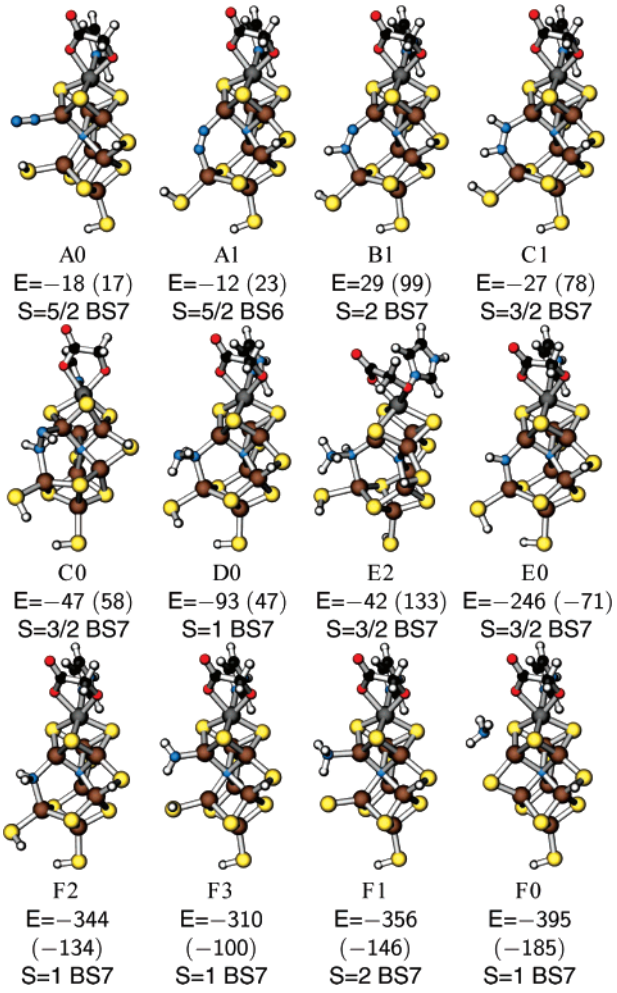

Figure 2. Intermediates of the main branch with their relative energies in kJ mol^{-1} and their spin state. The energies in parentheses are obtained with H_2 as a reference. B0 is not listed here because its access is considered kinetically hindered.[33] B0 corresponds to A1 with a protonated central ligand.

the frozen core approximation: Fe [Ne], Mo [Ar3d^{10}], S [Ne], O [He], N [He], C [He]. The following sets of projector functions were employed, Fe 2s2p2d, Mo 2s2p2d, S 2s2p2d, O 2s2p1d, N 2s2p1d, C 2s2p1d, H 2s1p, which provides the number of projector functions per angular momentum magnetic and spin quantum number (m,s) in each main angular momentum channel ⁄.

We considered the complete FeMoco with truncated ligands as shown in Figure 2. The histidine was replaced by imidazole, the homocitrate by glycolate, and the cysteine, bound to the terminal iron atom, by an SH group.

The atomic geometries were optimized using damped Car−Parrinello[47] molecular dynamics with all degrees of freedom relaxed. The convergence was tested by a microcanonical ab initio molecular dynamics simulation starting from the fully converged structure. No friction was applied to the atomic motion, and only a negligible friction has been used on the electronic wave functions. If the instantaneous temperature remained below 5 K during a simulation of 0.05 ps (200 time steps), the structure was considered converged.

The transition states were determined by applying a one-dimensional constraint on the atomic positions. In this application, bond length, angle, and torsion constraints were used. The specific constraint was varied continuously within 1000 MD steps to drag the system across the barrier. This approach provided a strict upper bound for the barrier

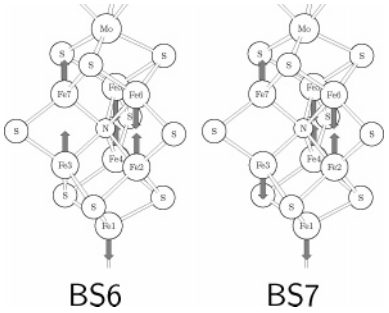

Figure 3. The two relevant spin orderings, BS6 and BS7. They differ by a spin flip of Fe3. BS7 is the same spin ordering as that obtained for the cofactor in the resting state M. It is characterized by ferromagnetically coupled Fe−Fe and Fe−Mo pairs, which are antiferromagnetically aligned relative to each other.[25] The spin ordering only defines the directions of the site spins not their absolute value.

height. If this upper bound was less than 20 kJ mol^{-1}, the resulting value was quoted as barrier height. Since barriers of this height are easily overcome within a turnover cycle, a more accurate determination would not provide relevant additional information. If, on the other hand, the first estimate of the barrier was higher than 20 kJ mol^{-1}, the value of the barrier height was refined further; the constraint was fixed to discrete values around the transition state to maximize the energy, while all unconstrained degrees of freedom were allowed to relax to minimize the energy. A proof that this approach, when converged, exactly determines first-order transition states is given elsewhere.[48]

The reaction rates Γ can be estimated using $\Gamma = \Gamma_0\, e^{-E_A/(k_B T)}$ from the calculated activation energy E_A and a typical attempt frequency $\Gamma_0 = 3 \times 10^{13}$ s^{-1} corresponding to about 1000 cm^{-1}, which is typical for a molecular stretch or bend vibration.

FeMoco has seven high-spin iron atoms antiferromagnetically coupled to each other. More precisely, in the resting state, we find four spin-paired transition-metal pairs, with an antiferromagnetic alignment of the pairs. Many different spin configurations may easily lead to metastable states in conventional collinear spin-polarized (UHF) calculations. Therefore, we used a noncollinear description of the spin density for our calculations. In a noncollinear description, each one-electron wave function is a two-component spinor wave function.[49−52] This method not only correctly describes the truly noncollinear spin states that occur within the reaction mechanism but also avoids the artificial barriers between different spin configurations occurring in collinear calculations. Our resulting spin distribution is, therefore, independent of the random starting conditions. Such dependence is a common problem of conventional (collinear) spin-polarized calculations for this system, which are easily trapped in metastable spin states. We found that the spin ordering depends on subtle changes in the atomic structure. The spin orderings encountered in our calculations are given in Figure 3, where we follow the notation introduced by Lovell et al.[53] Noncollinear spin arrangements have been found, in this study, only for energetically unfavorable states, which is why we do not specify them further.

The spin quantum number S is specified alongside the corresponding structures in Figures 2, 5, and 6. A spin with $S = 1$, for example, corresponds to a triplet.

During the reaction, protons and electrons are transferred to the cofactor and the substrate. We made the assumption that electrons and protons are coupled. This assumption implies one of two scenarios; either a reduction of the cofactor increases the proton affinity so that

(47) Car, R.; Parrinello, M. *Phys. Rev. Lett.* **1985**, *55*, 2471.
(48) Blöchl, P. E.; Togni, A. *Organometallics* **1996**, *15*, 4125.
(49) Sandratskii, L. M.; Guletskii, P. G. *J. Phys. F: Met. Phys.* **1986**, *16*, L43.
(50) Kübler, J.; Hock, K. H.; Sticht, J.; Williams, A. R. *J. Phys. F: Met. Phys.* **1988**, *18*, 469.
(51) Oda, T.; Pasquarello, A.; Car, R. *Phys. Rev. Lett.* **1998**, *80*, 3622.
(52) Hobbs, D.; Kresse, G.; Hafner, J. *Phys. Rev. B* **2000**, *62*, 11556.
(53) Lovell, T.; Li, J.; Liu, T.; Case, D. A.; Noodleman, L. *J. Am. Chem. Soc.* **2001**, *123*, 12392.

a proton transfer is induced, or, if the proton transfer precedes the electron transfer, the electron affinity is sufficiently enhanced by the positive charge next to the cofactor to induce an electron transfer to the cofactor. This is the main assumption in our work, besides the accuracy of the density functionals and the neglect of the protein environment, and it has been shown to be valid for the cofactor before binding of the substrate.[25]

The energies of the protons and electrons, which are consumed during the reaction, affect the overall reaction energy. It is common practice to express the energies relative to H_2 as the hydrogen source. However, the electrons and protons are not obtained from molecular hydrogen, and the reaction energies versus the energy of H_2 do not directly represent the biological system. The fact that H_2 is readily produced is a sign that H_2 is not in equilibrium with the particle reservoirs. Therefore, we define a chemical potential μ_H that reflects the biological environment. We used the formula $\mu_H = (1/2)E[H_2] + 35$ kJ mol^{-1}, which will be rationalized in the next paragraph. While the production of gaseous hydrogen, $2H^+ + 2e^- \rightarrow H_2$, is energetically neutral when using H_2 as a reference ($\mu_H = (1/2)E[H_2]$), as has been done in previous studies,[21,34,54−56] this reaction is exothermic by 71 kJ mol^{-1} when our μ_H is used. Additionally, we listed the reaction energies with H_2 as the reference energy in parentheses after the values we obtained with our μ_H.

Our choice of μ_H is rationalized by the following considerations.[25] For protons, the relevant particle reservoir is the proton transfer channel, while for electrons, it is expected to be the P cluster, a Fe_8S_7 cluster, which receives electrons from the Fe protein and passes them on to the FeMoco. The exact energies cannot be determined by theory alone. As a consequence of our assumption that reduction and protonation are coupled, only the sum μ_H of the energies of the protons and electrons is relevant for the relative energies of the intermediates. A range of possible values can be derived by comparing experimental X-ray and EXAFS data with our calculated geometries; we found indirect evidence that the cofactor is unprotonated in the resting state and is protonated in the reduced state.[25] Therefore, μ_H is sufficiently high to drive protonation, $\mu_H > E[MH] - E[M]$. On the other hand, no protonation occurs under the same conditions in the absence of MgATP. Thus, the chemical potential in the absence of MgATP, denoted by μ'_H, must be sufficiently low not to drive protonation, $\mu'_H < E[MH] - E[M]$. As two MgATP molecules are hydrolyzed in each electron transfer, the difference between the chemical potentials with and without MgATP is smaller than twice the energy of hydrolysis of MgATP, $\mu_H - \mu'_H < 64.4$ kJ mol^{-1}.[57] It is smaller because a fraction of the energy supplied by MgATP will be dissipated. Therefore, we use the lower bound for μ_H, which is $\mu_H = E[MH] - E[M]$, in our calculations. This is the most conservative assumption possible. A less conservative value would make those reactions that include protonation more exothermic.

In this work, we evaluate not only the energetics of the intermediates but also the barriers for the transitions. This is not problematic for intramolecular rearrangements. However, to estimate the barriers for protonation, we need to simulate the proton channel. We used an ammonium molecule to mimic the proton donor. This choice only affects the barriers, not the relative energies of the intermediates.

3. Results

An overview of the reaction cycle is given in Figure 4. The geometric structures of the intermediates and their energies are shown in Figures 2, 5, and 6. Let us first define our notation for the intermediates: The resting state of the cofactor is denoted by M. After *n* protonation and reduction steps, the cofactor is denoted by MH*n*. The cofactor MH2 with dinitrogen bound is denoted as A*i*, where the numeral *i* is a label that orders the different metastable configurations according to increasing energy. A numeral 0 denotes the ground state for the selected composition. The reaction is driven by repeated protonation and reduction steps. After each protonation−reduction step, we step the letter forward in the alphabet to obtain B*i*, C*i*,...,F*i*.

The reaction path has been determined as follows. We exploited the experimental fact that the electron transfer to the cofactor is the rate-limiting step of biological nitrogen fixation (see Introduction). Starting from a particular intermediate, we initiated a reaction sequence by adding an electron. Then we tried possible protonation sites until we found the most favorable protonation site. Interestingly, the intermediates usually offer only a single proton acceptor. Following protonation, we investigated possible rearrangements of the system by calculating the reaction energies and the reaction barriers until we reached the global minimum. The biological system rests in this state until the next electron is delivered from the Fe protein. Thus, we repeated the steps described, beginning with electron and proton transfer. An important aspect of our work is to determine the reaction by excluding unproductive side reactions. This is why we also mention the side branches encountered in this study.

Previously,[25,33] we traced the reaction mechanism from the resting state to the protonation of dinitrogen bound to the FeMoco. Already, before dinitrogen is protonated, there are two coexisting binding modes, namely, the axially bound dinitrogen A0 and the dinitrogen bridging two Fe atoms, A1. They are shown in Figure 2. As shown in Table 1, the axial binding mode is more stable by 6 kJ mol^{-1}. The two states are separated by a large barrier, which, however, is still sufficiently small to be overcome within a turnover cycle. Upon reduction, the energetic order of the two states is interchanged, making the pathway via the bridged configuration more favorable. Following protonation, we find the bridged dinitrogen, B1, 19 kJ mol^{-1} lower in energy than the axially bonded one, represented by B2 (see Table 1 and Figure 5). This is the reason why we argue that the main pathway proceeds via the bridged configuration A1. Nevertheless, side branch 1 will also be considered.

Another side branch, namely, side branch 2, will not be discussed in this paper because it has already been discussed in detail before.[33] While it passes through a more stable intermediate than the other pathways, this intermediate B0 with a protonated central ligand is only accessible via a barrier too large to be overcome during a turnover cycle.

The third side branch that will be discussed in this paper is side branch 3, which appears to be a dead alley.

In the following, we will discuss the reactions starting with the main branch.

3.1. Main Branch. Figure 7 shows a profile of the reaction energy of the main branch. The vertical or curved arrows indicate reduction by one electron and subsequent protonation. After reduction, the proton is first added to an ammonia. If, on the one hand, the system with ammonium is metastable, a vertical arrow is drawn to the energy of the intermediate with the proton still residing on the donor. If, on the other hand, the proton transfer from ammonium to the substrate is spontaneous, a curved arrow is drawn to the resulting intermediate.

(54) Rod, T. H.; Hammer, B.; Nørskov, J. K. *Phys. Rev. Lett.* **1999**, *82*, 4054.
(55) Rod, T. H.; Nørskov, J. K. *J. Am. Chem. Soc.* **2000**, *122*, 12751.
(56) Rod, T. H.; Logadottir, A.; Nørskov, J. K. *J. Chem. Phys.* **2000**, *112*, 5343.
(57) Voet, D.; Voet, J. G.; Pratt, C. W. *Lehrbuch der Biochemie*; John Wiley & Sons: New York, 2002.

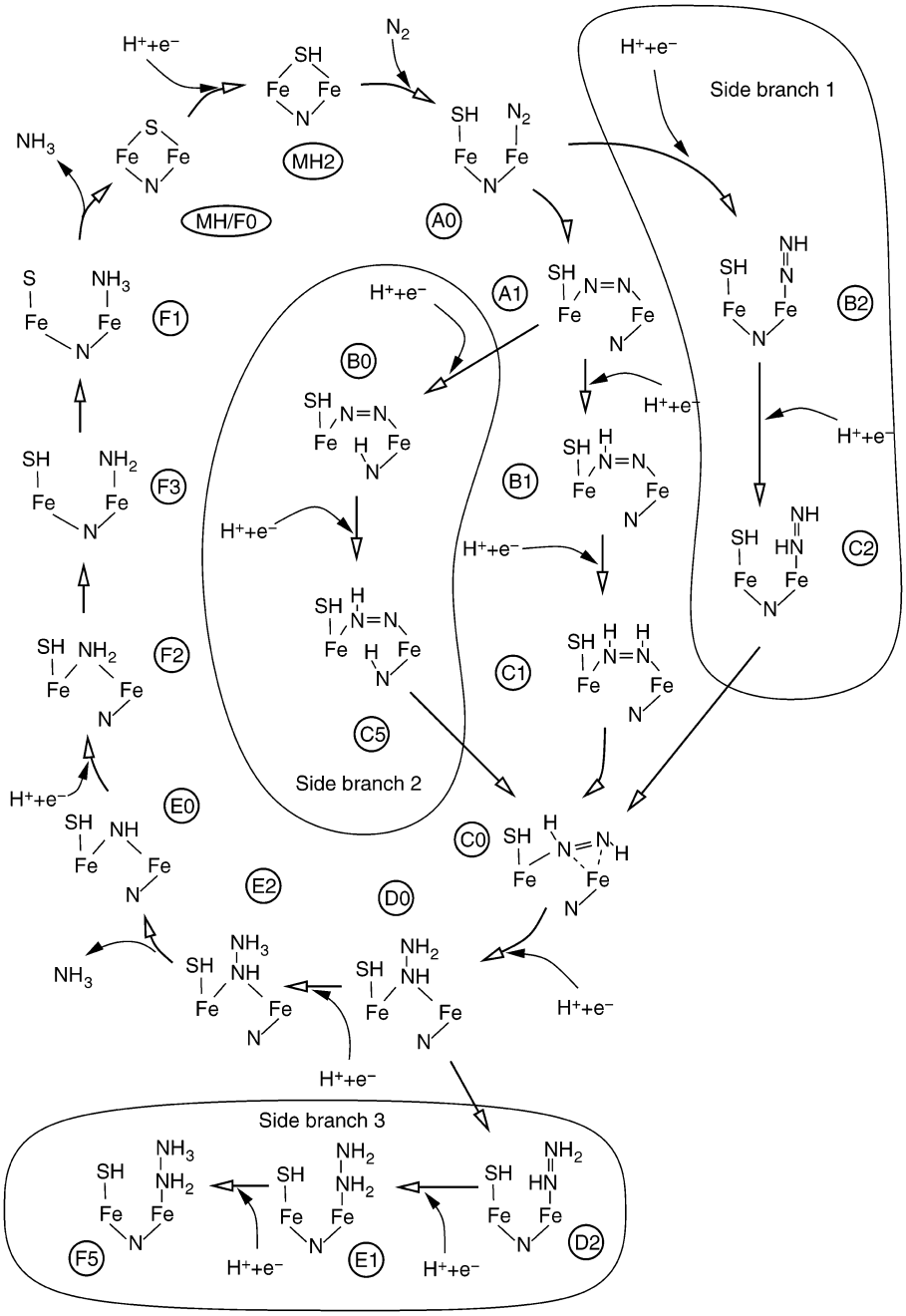

Figure 4. Scheme of the main branch and the three side branches discussed in the text. The cycle passing through B1 and C1 is the main branch. Side branch 1 passes through B2 and C2. Side branch 2 passes through B0 and C5. The unproductive side branch 3 separates from C0 via D2 and E1−F5. The schemes show the two Fe atoms of the central cage and the sulfur atom bridging them in the resting state. The nitrogen atom common to all intermediates is the central ligand of the FeMoco.

As the reactions leading to the first protonation of dinitrogen have been discussed in an earlier paper, we start with the second protonation of dinitrogen.

3.1.a. Second Protonation of Dinitrogen. In B1, one of the protonation sites of N_2 has been saturated; thus, there is only one protonation site left, namely, the one on the unprotonated N atom. Following reduction, B1 is spontaneously protonated by NH_4^+. Note that we model the proton transport channel by a single ammonium, as rationalized in the Computational Details. The resulting structure C1 contains a *cis*-diazene (H−N═N−H) fragment. In Table 2, the geometrical data of C1 are compared to other diazene adducts of the nitrogen fixation cycle.

The *cis* form, C1, is only metastable and converts into the more stable *trans* form, C0. The reaction is exothermic by 20 kJ mol^{-1} and has a barrier of 26 kJ mol^{-1}. In this structure, *trans*-diazene forms a π complex bond with one Fe atom, while another Fe atom saturates one of its lone pairs.

C0 is common to all branches discussed in this paper.

3.1.b. Third Protonation. In C0, diazene has only a single proton acceptor site available, namely, on the nitrogen atom *trans* to the Fe−N σ bond.

Following reduction and protonation, C0 converts into the σ complex D0. Here, the distal nitrogen atom is part of an NH_2 group connected to the proximal one, which is tetrahedrally

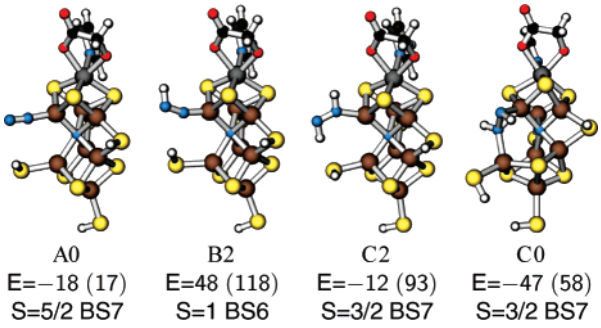

Figure 5. Intermediates of side branch 1: protonation of axial dinitrogen (A0) with their relative energies in kJ mol^{-1} and their spin state. The energies in parentheses are obtained with H_2 as a reference.

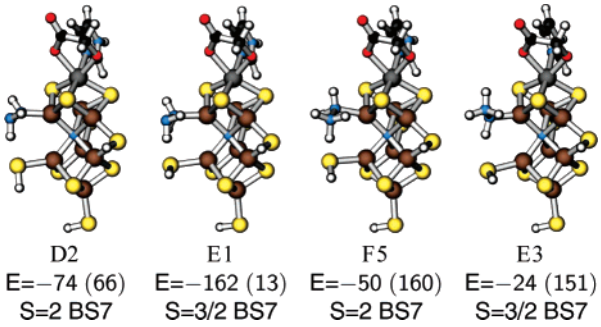

Figure 6. Intermediates of side branch 3 with their relative energies in kJ mol^{-1} and their spin state. The energies in parentheses are obtained with H_2 as a reference. The substrate is bound as Fe−NH−NH_2 in D2, as Fe−NH_2−NH_2 in E1, as Fe−NH_2−NH_3 in F5, and as Fe−NH−NH_3 in E3.

Table 1. Energies in kJ mol^{-1} of the Intermediates of the Main Branch Relative to MH, Free N_2, Free NH_3, and Our Choice of μ_H Rationalized in Computational Details[a]

state	H	NH_3	E_{rel}	
M	0	0	0	(−35)
MH	1	0	0	(0)
MH2	2	0	13	(48)
A0	2	0	−18	(17)
A1	2	0	−12	(23)
B1	3	0	29	(99)
C1	4	0	−27	(78)
C0	4	0	−47	(58)
D0	5	0	−93	(47)
E2	6	0	−42	(133)
E0	6	1	−246	(−71)
F2	7	1	−344	(−134)
F3	7	1	−310	(−100)
F0	7	1	−395	(−185)

[a] Relative energies with H_2 as a reference are given in parentheses.

Table 2. Geometry of Intermediates Containing Diazene[a]

	C0	C1	C2
N−N	1.396	1.346	1.291
N_1−H	1.043	1.035	1.043
N_2−H	1.036	1.037	1.059
N_1−Fe7	1.942	1.888	1.889
N_2−Fe7	2.004		
N_2−Fe3	2.072	1.934	
N_2−N_1−Fe7	71.7	128.9	145.0
H−N−N−H	160.9	5.4	179.0

[a] Distances are given in angstroms and angles in degrees. N_1 refers to the uppermost nitrogen atom in Figures 2 and 5.

coordinated by two Fe atoms, one proton, and the distal N atom. During this protonation, the N═N double bond of C0 is converted into a single bond.

The intermediate C0 can be bypassed; C1 can directly be converted into D0. This reaction, however, requires that the system is reduced before the barrier from C1 to C0 has been overcome. Thus, it will only occur at high electron flux. In this case, the third proton is added to either of the two nearly equivalent nitrogen atoms of C1. The reaction of the protonated C1 to D0 is exothermic by 18 kJ mol^{-1}.

3.1.c. Fourth Protonation. Protonation of the only lone pair of structure D0, namely, the one at the distal NH_2 group, requires only a small barrier of 11 kJ mol^{-1} using ammonium as a proton donor. It results in the high-energy intermediate E2 with a rather long, but still intact, N−N bond.

From E2, shown in Figure 2, an ammonia molecule is easily dissociated, leading to structure E0. The barrier to cleave the N−N bond is only <10 kJ mol^{-1}, and the reaction is strongly exothermic with 204 kJ mol^{-1}.

3.1.d. Fifth Protonation. Protonation of the intermediate E0 at the bridging NH group is spontaneous, using ammonium as the proton donor, and leads to F2, shown in Figure 2.

F2 does not have proton acceptor sites at nitrogen. In order to expose a lone pair, one Fe−N bond must break, leading to F3. While this Fe−N bond is broken, one Fe−N bond to the central ligand is restored so that the number of bonds is preserved. In this step, the central ligand completes its coordination shell, as shown in Figure 2. This step is endothermic by 34 kJ mol^{-1} and has a barrier of 45 kJ mol^{-1}.

In order to investigate the sequence of the bond-forming and bond-breaking processes, we investigated the two-dimensional energy surface, shown in Figure 8. Here, the total energy is calculated as a function of the bond lengths of the two Fe−N bonds, the one to the central ligand and the one to the nitrogen originating from dinitrogen. Each point corresponds to a state where both bond lengths are fixed to the corresponding values, while all other degrees of freedom were fully relaxed.

The energy surface exhibits a third local minimum, namely, F4. In F4, both bonds are broken. Its energy lies 56 kJ mol^{-1} above that of F2 and 11 kJ mol^{-1} above the direct transition state from F2 to F3. Both transition states lie, energetically, 62 kJ mol^{-1} above F2. Thus, we conclude that this indirect path is unfavorable, and the bond breaking and bond formation occur in a concerted fashion, that is, via TS1.

3.1.e. Sixth Protonation: Final Ammonia Detachment. In the intermediate F3, NH_2 exposes one lone pair, which is readily protonated.

The most favorable pathway proceeds via an intramolecular proton transfer from the SH group and results in F1. The proton transfer has a negligible barrier and is exothermic by 46 kJ mol^{-1}. The singly coordinated sulfur atom completes its coordination by restoring the sulfur bridge between the Fe sites. As this happens, ammonia is dissociated in a concerted fashion. Also, this second reaction step has a negligible barrier and is exothermic by 39 kJ mol^{-1}. It leads to MH and thus closes the catalytic cycle.

As no external proton or electron transfer is required to proceed from F2 to F0, the corresponding steps do not have to wait for any Fe protein cycles to finish. All of them appear as one step in the Thorneley−Lowe scheme.

We considered also a side branch from F3 to MH2 proceeding via reduction of the cofactor in structure F3 followed by an

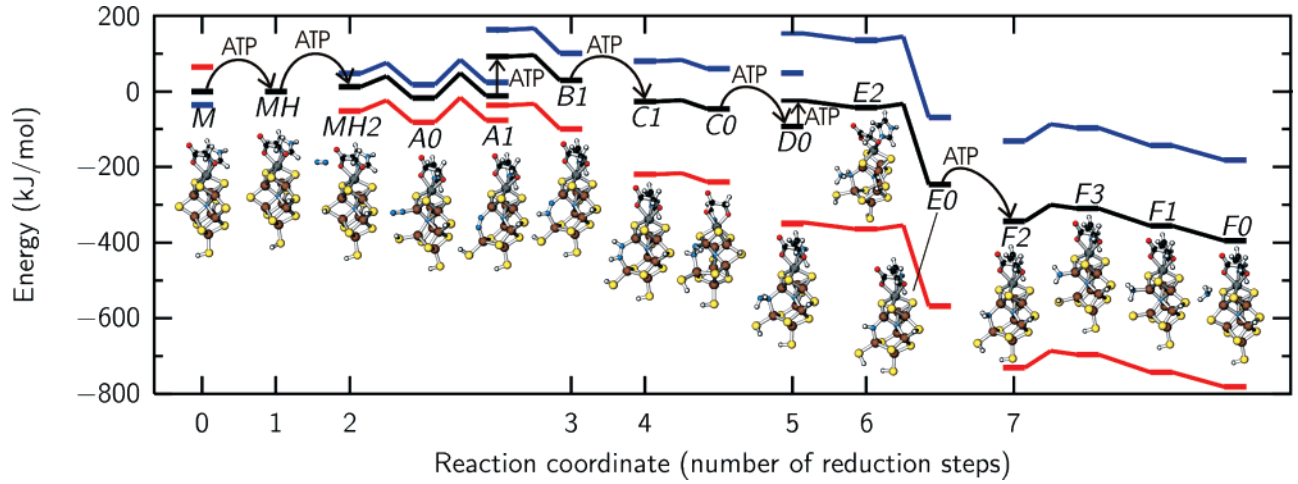

Figure 7. Energy profile of the main branch of dinitrogen conversion from the resting state and free N_2 to the second NH_3 abstraction. Each arrow indicates a coupled reduction and protonation step. The energies for such steps depend on μ_H. The black curve is the energy profile with our choice of μ_H, the blue curve corresponds to $\mu_H = (1/2)E[H_2]$, and the red curve assumes that all of the energy of ATP hydrolysis is used for the reduction of the FeMoco. According to our calculations, the range between the black and the red line represents the biological reaction.

Table 3. Energies Relative to F2 and Geometries of Intermediates and Transition States Involved in a Rearrangement after the Fifth Protonation

state	energy kJ mol^{-1}	d(N–Fe$_3$) Å	d(N$_x$–Fe$_3$) Å
F2	0	2.094	3.340
F3	34	3.587	2.031
F4	56	4.061	3.944
TS1	45	2.841	2.134
TS2	62	3.368	3.770
TS3	62	3.820	3.119

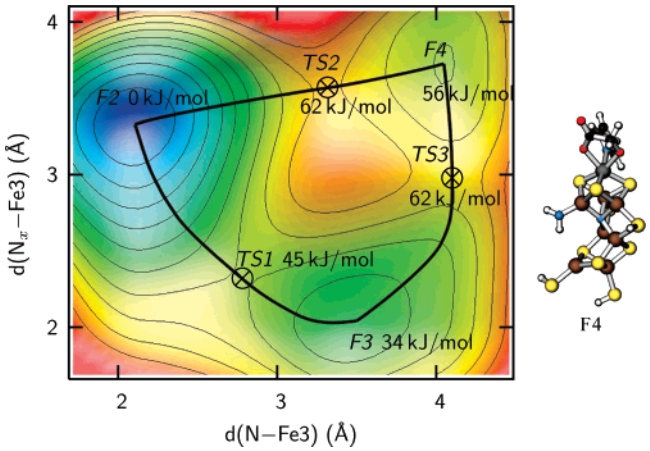

Figure 8. Schematic contour plot of the energy surface for a rearrangement after the fifth protonation, the transition from F2 (upper left) to F3 (bottom right). The d(N−Fe3) is the distance between N of the NH_2 group and Fe3. The d(N$_x$−Fe3) is the distance between the central ligand and Fe3. The values for the distances are given in Table 3. The energies are given relative to the starting state of this step, F2.

external proton transfer. Also, this protonation from ammonium as the proton donor proceeds easily. However, the resulting NH_3 ligand is quite strongly bound to Fe. While dissociation is exothermic by 46 kJ mol^{-1}, it has a large barrier of 72 kJ mol^{-1}, which would be the highest barrier in the whole process. Thus, we conclude that this side branch is not relevant. Following dissociation of NH_3, the SH group reconnects to the second Fe, leading to MH2, which is the final point and the starting point of the catalytic cycle.

3.2. Side Branch 1. As discussed previously,[33] the first protonation of N_2 may be performed not only in the bridging structure A1 but also in the axial binding mode A0. Protonation of A0 leads to B2, shown in Figure 5. The energetics of side branch 1 are presented in Figure 9.

3.2.a. Second Protonation. The second proton attaches to the proximal atom of the axially bound dinitrogen, resulting in the *trans*-diazene adduct C2, shown in Figure 5. Protonation of the distal nitrogen atom, which is already protonated, is unfavorable by 43 kJ mol^{-1}.

C2 is only a metastable intermediate; a rotation of diazene leads to the π complex C0. This transformation from C2 to C0 is exothermic by 35 kJ mol^{-1} and has a barrier of 44 kJ mol^{-1}.

At this point, the side branch 1 has a common intermediate with the main branch discussed earlier, namely, C0. Thus, the two branches of the catalytic cycle join here.

The side branch 1 may extend to D0 if the transformation from C2 to C0 is not completed before the next proton is added. If the next electron transfer proceeds while the system still resides in C2, it can be directly protonated at the distal nitrogen atom, resulting in D2. Intercalation of the proximal nitrogen atom between the two Fe atoms, leading to D0, is exothermic by 19 kJ mol^{-1} and requires only a small barrier of <12 kJ mol^{-1}.

3.3. Side Branch 3: From D0 to E1. While we consider this side branch as unfavorable, it shall be described here for sake of completeness and because this alternative side branch is analogous to a pathway suggested earlier.[34,54−56] Differing from that work, however, here, we consider the SH bridge to be open. Starting from D0, the system can break one Fe−N bond and convert into D2, having axially bound NH−NH$_2$, as shown in Figure 6. D2 is 19 kJ mol^{-1} higher in energy than D0, as illustrated in Figure 10 and is, therefore, populated with lower probability.

Reduction and protonation of D2 at the proximal nitrogen atom leads to E1, shown in Figure 6, a hydrazine bound head-on to one Fe site. Protonation at the terminal nitrogen leading to E3 can be excluded because it requires 138 kJ mol^{-1} more energy than protonation at the proximal nitrogen leading to E1. In E1, however, the system is trapped; the next reduction and

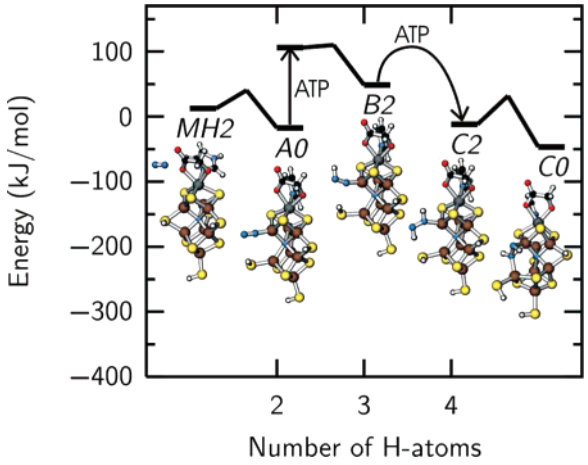

Figure 9. Energy scheme of side branch 1: protonation of axial dinitrogen (A0). See Figure 7 for details.

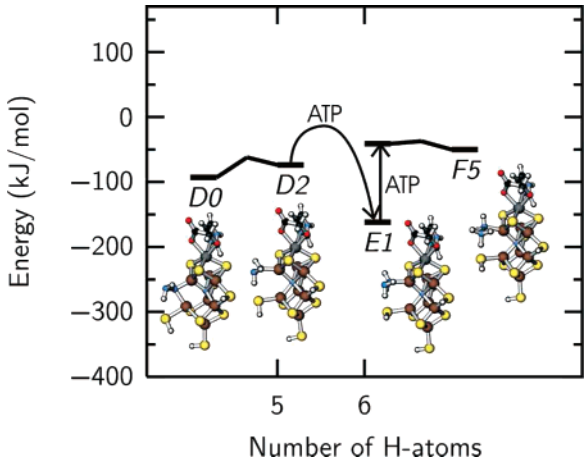

Figure 10. Energy scheme of side branch 3. As protonation of E1 is energetically unfavorable, the system would be trapped in E1 and possibly react back. See Figure 7 for details.

protonation step leads to the unfavorable intermediate F5. The additional proton, however, is not stable on hydrazine in the presence of an ammonia. It can only be stabilized if ammonia is completely isolated structurally, preventing it from forming any other hydrogen bonds. If the protonated hydrazine bound to the cofactor is even unstable in the gas phase, it can be expected to be even less stable in the protein environment. Therefore, we expect the system to be trapped for a long time in E1 and to react back via D2 to D0.

With the exception of E1, all intermediates of this side branch are higher in energy than those of the main branch. E1 is 120 kJ mol^{-1} more stable than E2 and 84 kJ mol^{-1} less stable than E0, into which E2 transforms. The intermediate F5 of the side branch, however, is 294 kJ mol^{-1} higher in energy than F2 of the main branch. Thus, we conclude that this branch is not relevant.

4. Discussion

Our study exhibits a main branch and several side branches. The thorough investigation of productive and unproductive side reactions sets our study apart from earlier simulations. This approach provides additional confidence for two reasons. First, we compare competing mechanisms with the same methodology, which minimizes errors. Second, the qualitative picture is

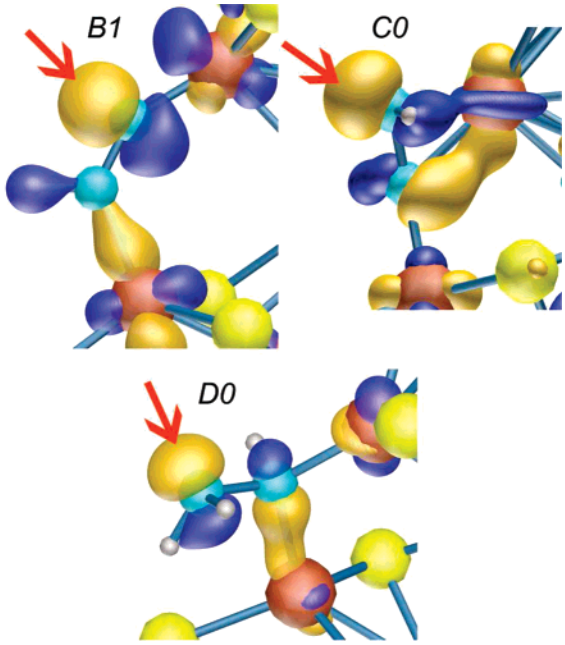

Figure 11. Occupied one-electron wave functions (orbitals) with arrows pointing to the lone pairs to be protonated. Top left: B1 (+4.20 eV). Top right: C0 (+2.47 eV). Bottom: D0 (+2.39 eV). In all cases, these orbitals have π^* contributions to the N−N bond. The contours are shown for 0.04 electrons a_B^{-3} in the top graphs and 0.06 electrons a_B^{-3} for D0.

determined by rather large energy differences. It is the fact that a particular intermediate or barrier has a very high energy that limits the configuration space accessible during the reaction. Thus, we believe that our main conclusions are fairly robust with respect to the limitations of our theory.

In the following, we place the different side reactions into perspective.

One of the side branches, branch 3, is a dead alley and needs not be considered any further. While this branch is very intuitive and closely related to a widely discussed model based on axially bound nitrogen, we find that the complete protonation of the terminal nitrogen requires a prohibitive energy cost. The energy cost is sufficiently large that we are confident that this qualitative result is unaffected by the accuracy of our methodology.

The situation is different for side branches 1 and 2. According to our calculations, the main branch is favored. The relevant energy differences that discriminate the main branch from branches 1 and 2 lie near 20 kJ mol^{-1}. Deviations of our theory from experiment of this magnitude are unlikely, given the chemical similarities of the competing intermediates, but they cannot be excluded with certainty.

As discussed earlier, the argument used to exclude side branch 2 is stronger, as it is based on a fairly large kinetic barrier to form B0. Nevertheless, it is striking that the catalytic cycle does not pass through an intermediate with lower energies at this composition. It also should be taken into account that the density functionals used in the study do not reproduce barriers with the same accuracy as the energies of intermediates.

However, side branch 1 must be considered a viable alternative to the main branch. Here experiment or more accurate calculations may be able to give more confidence in one or the other pathway. Nevertheless, also this side branch differs from the main branch only by two intermediates.

Most of the reaction, in particular the dissociation of ammonia, seems to proceed by a well-defined pathway.

4.1. How the Electronic Structure Directs Protonation. After the first protonation, it is a common motive of the reaction mechanism that the species to be protonated has an asymmetric N−N bond. This directs protonation to a specific N site. Lone pairs to be protonated are shown in Figure 11. While a reduction, which we assume to be necessary for the protonation, makes the protonation energetically more favorable, the lone pairs are already occupied before the reduction.

4.2. Required Properties of the Cofactor. Flexibility of the cofactor is important for catalyzing the reaction steps discussed in this work. Differently sized intermediates of protonated dinitrogen have to be bound by the cofactor. We find states where two of the Fe atoms are bridged by a sulfur bridge, by a dinitrogen bridge, or by a single nitrogen atom. The cofactor allows the distance of the Fe atoms to be varied from 2.556 Å in the resting state via 3.441 Å in D0 to 4.250 Å in A1. The cavity in the protein provides sufficient space for the opening of the SH bridge.[25] While sulfur prefers a bond angle close to or even smaller than 90°, nitrogen prefers an angle closer to the tetrahedral angle of 109°, as in D0. This change can be accommodated best if site Fe3 is pulled out of the cluster. This movement of Fe3 is made possible by cleaving its bond to the central ligand.

The cofactor is not only flexible in a geometric sense, but it may also act as an electron sponge. Cleavage of the N−N bond requires the transfer of two electrons with antiparallel spins from the cofactor to dinitrogen. This is facilitated by a large cluster with a delocalized electron system because the change of the average oxidation state is smaller than in a small metal cluster. The electron pair consists of one spin-up and one spin-down electron. A single high-spin Fe atom can only provide electrons with parallel spin. In the FeMoco, dinitrogen is in direct contact with two Fe sites with antiparallel spins, which can supply an electron pair with antiparallel spin.

Also, the final reaction step, namely, the dissociation of the second ammonia from F2, relies on the special features of the cofactor; it would have one of the largest barriers in the mechanism if the sulfur bridge would not be restored. The dissociation of the ammonia is part of a substitution reaction in which the coordination number of the Fe atom is restored by the sulfur atom as soon as ammonia leaves.

4.3. Dependence of Our Results on the Choice of the Hydrogen Chemical Potential. As pointed out in section 2, the energy profile depends on the choice of the chemical potential for protons and electrons, which are combined in μ_H. Note that only the energies of those reaction steps, for which the number of hydrogen atoms changes, are affected by the choice of μ_H. We have chosen a value for μ_H based on a comparison of our calculations with experiment. Nevertheless, there is a large uncertainty in the chosen value. To relate our results to other calculations, it is necessary to understand how the results depend on μ_H.

The energy of each protonation step and thus the reaction energy of the entire nitrogen reduction cycle depend on the hydrogen chemical potential μ_H. This value cannot be obtained from calculations, as it depends on the chemical environment, the pH value, the reduction potential, and other properties in the vicinity of the cluster.

A value for μ_H may be obtained from the experimental reaction energy of the entire cycle. However, previous estimates differ substantially depending on the assumptions made in the analysis.

Alberty[58] approximated the standard Gibbs energy for N_2 conversion with $\Delta_r G^\circ = -463.18$ kJ mol^{-1} for the chemical reaction defined via one specific set of educts and products (ferredoxin with a reduction potential of −0.403 V, H^+, NH_4^+).

For the biochemical equation defined for equilibrium concentrations of H_3O^+/H_2O and NH_4^+/NH_3 at pH = 7 with the same ferredoxin, he obtained[58] the transformed Gibbs energy, $\Delta_r G'^\circ = -63.62$ kJ mol^{-1}.

We rationalized the choice of μ_H used in the present work, assuming $\Delta_r E = 0$ for the first reduction and protonation of the resting state. This choice of μ_H leads to $\Delta_r E = -395$ kJ mol^{-1} for the whole reaction. The Gibbs free energy is related to the calculated reaction energy by $\Delta_r G = \Delta_r U - T\Delta_r S + \Delta_r(pV)$ with $\Delta_r U \approx \Delta_r E$.

Most previous calculations chose the chemical potential μ_H equal to one-half of the energy of a hydrogen molecule, which is 35 kJ mol^{-1} below our choice for μ_H and leads to a reaction energy of $\Delta_r E = -185$ kJ mol^{-1}.

5. Summary

We studied cleavage of the N−N bond of dinitrogen at the FeMo cofactor on the basis of density functional calculations. We made an effort to explore the phase space for the reaction without prejudice for one particular model of the mechanism. A large number of intermediates and the barriers between them have been explored and placed into perspective. Three branches emerged from this procedure. However, they join before the N−N bond is broken. A fourth branch was found but is unlikely to play a role in the reaction cycle due to high-energy intermediates. Cleavage of the N−N bond is facilitated by the flexible geometric and electronic properties of the cofactor. We provided a rationalization of the mechanistic features relevant to accomplish critical reaction steps, which may be useful to develop model systems for nitrogen fixation.

Acknowledgment. We acknowledge support by the HLRN for granting access to their IBM pSeries 690 supercomputers.

Supporting Information Available: Calculational details (PDF). This material is available free of charge via the Internet at http://pubs.acs.org.

JA068618H

(58) Alberty, R. A. *J. Biol. Chem.* **1994**, *269*, 7099.